

# Enhancing Industrial X-ray Tomography by Data-Centric Statistical Methods

Jarkko Suuronen<sup>1</sup>, Muhammad Emzir<sup>2</sup>, Sari Lasanen<sup>3</sup>, Simo Särkkä<sup>2</sup> and Lassi Roininen<sup>1\*</sup>

<sup>1</sup>School of Engineering Science, Lappeenranta-Lahti University of Technology, PO Box 20, FI-53851 Lappeenranta, Finland.

<sup>2</sup>Department of Electrical Engineering and Automation, Aalto University, PO Box 11000, FI-00076 Aalto, Finland. <sup>3</sup>Sodankylä Geophysical Observatory, University of Oulu, PO Box 8000, FI-90014 University of Oulu, Finland.

\*Corresponding author. E-mail: [lassi.roininen@lut.fi](mailto:lassi.roininen@lut.fi)

(Received xx xxx xxxx)

**Keywords:** Bayesian statistical inverse problems; non-Gaussian random fields; contrast-boosting inversion; Hamiltonian Monte Carlo; industrial X-ray tomography

## Abstract

X-ray tomography has applications in various industrial fields such as sawmill industry, oil and gas industry, chemical engineering, and geotechnical engineering. In this article, we study Bayesian methods for the X-ray tomography reconstruction. In Bayesian methods, the inverse problem of tomographic reconstruction is solved with help of a statistical prior distribution which encodes the possible internal structures by assigning probabilities for smoothness and edge distribution of the object. We compare Gaussian random field priors, that favour smoothness, to non-Gaussian total variation, Besov, and Cauchy priors which promote sharp edges and high-contrast and low-contrast areas in the object. We also present computational schemes for solving the resulting high-dimensional Bayesian inverse problem with 100,000-1,000,000 unknowns. In particular, we study the applicability of a no-U-turn variant of Hamiltonian Monte Carlo methods and of a more classical adaptive Metropolis-within-Gibbs algorithm for this purpose. These methods also enable full uncertainty quantification of the reconstructions. For faster computations, we use maximum a posteriori estimates with limited-memory BFGS optimisation algorithm. As the first industrial application, we consider sawmill industry X-ray log tomography. The logs have knots, rotten parts, and even possibly metallic pieces, making them good examples for non-Gaussian priors. Secondly, we study drill-core rock sample tomography, an example from oil and gas industry. We show that Cauchy priors produce smaller number of artefacts than other choices, especially with sparse high-noise measurements, and choosing Hamiltonian Monte Carlo enables systematic uncertainty quantification.

## Impact Statement

Industrial X-ray tomography reconstruction accuracy depends on various factors, like the equipment, measurement geometry and constraints of the target. For example dynamical systems are harder targets than static ones. The harder and noisier the setting becomes, the more emphasis goes on mathematical modelling of the targets. Bayesian statistical inversion is a common choice for difficult measurement settings, and its limitations mainly come from the choice of the a priori models. Gaussian models are widely studied, but they provide smooth reconstructions. Total variation priors are not invariant under mesh changes, so doing systematic uncertainty quantification, like data-centric sensor optimisation, cannot be done with them. Besov and Cauchy priors however provide systematic non-Gaussian random field models, which can be used for contrast-boosting tomography. The drawback is higher computational cost. Hence, the techniques developed here are useful for non-time-critical applications with difficult measurement settings. In these cases, the methods developed may provide significantly better reconstructions than the traditional methods, like filtered back-projection.

## 1. Introduction

X-ray tomography has applications in various industrial fields such as sawmill industry, where it can be used for detecting knots, rotten parts and foreign objects in sawmills (Shustrov *et al.*, 2019; Zolotarev *et al.*, 2019). In oil and gas industry, X-ray tomography can be used to analyze drill-core rock samples to identifying pore structures (Mendoza *et al.*, 2019) and other structural properties of rock. In chemical engineering, X-ray microtomography can be used to measure the internal structure of substances at the micrometer level (Ou *et al.*, 2017). In manufacturing it can be used in nondestructive testing (Garcea *et al.*, 2018; Rotella *et al.*, 2018), endurance testing (Piao *et al.*, 2019), and dimensional metrology (Kruth *et al.*, 2011; Villarraga-Gómez *et al.*, 2019). In geotechnical engineering, X-ray microtomography can be used to measure soil properties in laboratories, while a closely related travel-time tomography can be used to measure the structure of soil and rocks from cross-borehole measurements (Ernst *et al.*, 2007; Huai *et al.*, 2016).

The principle of X-ray tomography is that we transmit X-ray radiation to the object, which penetrates the object of interest over a collection of propagation paths, and the attenuated X-ray radiation is measured in a detector system (Toft, 1996). This allows us to estimate internal properties of an unknown object given the noise-perturbed indirect measurements. However, typically, we can transmit and measure the X-rays only from a limited number of angles around the object which makes it harder to reconstruct the internal structure of the object from the measurements. The reconstruction problem is thus an inverse problem where the measurements give only a limited amount of information on the object of interest (Siltanen *et al.*, 2003).

In order to successfully reconstruct the internals of the object from the limited number of measurements, we need to introduce additional information to the reconstruction process. In this article, we study so-called Bayesian methods (Kaipio and Somersalo, 2005), where we introduce a statistical prior model for the possible internal structures in form of a probability distribution. This prior model encodes the information on what kind of structures are more likely and which are less likely than others. For example, a Gaussian random field prior puts higher probability for smoother structures whereas total variation (TV), Besov, and Cauchy priors favor structures that can have sharper edges between the substructures (González, 2017). The advantage of the Bayesian formulation is that it provides uncertainty quantification mechanism to the reconstruction problem, as it not only provides single reconstruction, but also the error bars for the reconstruction in form of a probability distribution (Bardsley, 2012).

The Bayesian formulation of the X-ray tomography problem transforms the solution to the associated inverse problem to a Bayesian inference problem, where we need to use computational methods from Bayesian statistics to solve it. In this article, we use Markov chain Monte Carlo (MCMC) methods, and in particular, Metropolis-within Gibbs (MwG) sampling and Hamiltonian Monte Carlo (HMC) which are powerful tools for this purpose. We also experiment simpler solution methods which find the maximum posterior probability reconstructions (maximum a posteriori, MAP, estimates) by using numerical optimization.

In the experiments we concentrate on two industrial problems. The first one is sawmill industry application, doing log tomography for detecting knots, rotten parts and foreign objects in sawmills (Shustrov *et al.*, 2019; Zolotarev *et al.*, 2019). The second application is drill-core rock sample tomography, in oil and gas industry, for identifying pore structures (Mendoza *et al.*, 2019).

### 1.1. X-ray tomography as a Bayesian statistical inverse problem

In general, reducing the number of measurements tends to add artefacts to the tomographic reconstruction. This means that we need to carefully evaluate the accuracy of the reconstruction for different levels of sparsity. For this kind of problems, a typical approach is to deploy Bayesian statistical inversion

techniques in the sense of [Kaipio and Somersalo \(2005\)](#). Bayesian inversion is the theory and practical data analysis of noisy indirect measurements within the Bayesian estimation framework. Following [Toft \(1996\)](#), X-ray radiation measured at single detector pixel over a given propagation path is

$$y_{\theta,s} = \iint X(x_1, x_2) \delta(s - x_1 \cos \theta - x_2 \sin \theta) dx_1 dx_2 + e_{\theta,s} =: \mathcal{A}_{\theta,s} X + e_{\theta,s}, \quad (1)$$

where  $y_{\theta,s}$  is measured value at angle  $\theta$  with translation  $s$  and  $X$  is varying X-ray attenuation coefficient field inside the object of interest. For practical computations, we discretise the operation  $\mathcal{A}_{\theta,s} X$  by approximating  $X$  with a piecewise defined function with constant values on square pixels, and obtain a finite-dimensional presentation  $y = AX + e$ , where  $y \in \mathbb{R}^n$ ,  $A \in \mathbb{R}^{n \times m}$ ,  $e \in \mathbb{R}^n$ , and  $X \in \mathbb{R}^m$  represent the approximated values of  $X$  on pixels.

In X-ray tomography, the noise process  $e$  is often modelled as a compound Poisson distributed noise ([Whiting, 2002](#); [Thanh et al., 2019](#)). We make a simplification, and assume that  $e$  is zero-mean Gaussian white noise with covariance  $C = \sigma^2 I$ . As our main aim is in contrast-boosting priors, so we assume that this simplification does not affect the generality of the results. The solution of the tomography problem is then an a posteriori probability density via the Bayes formula

$$\pi(X|y) = \frac{\pi(X) \pi(y|X)}{\pi(y)} \propto \pi(X) \pi(y|X) = \pi(X) \exp\left(-\frac{1}{2} (y - AX)^T C^{-1} (y - AX)\right), \quad (2)$$

where  $\pi(X)$  is the a priori density, that is, the probabilistic description of the unknown we know before any measurements are taken,  $\pi(y|X)$  is the likelihood density, and  $\pi(y)$  is a normalizing constant, which we shall omit, as we carry out computations by using unnormalized densities.

## 1.2. Literature review

Sparse-angle tomography is an ill-posed inverse problem ([Natterer, 2001](#)), and thus in order to have stable solutions, we need to set the prior  $\pi(X)$ . As our objective is in reconstructing unknown objects with sharp interfaces, which are often referred as edges, we need to choose a prior density that can model the edges. A standard choice is to use Gaussian random field priors ([Bardsley, 2013](#)). They are easy to use through their analytic properties, that is, they are fully defined by their means and covariances. The drawback of Gaussian priors is that they are locally smoothing, and thus cause contrast artefacts near sharp edges. Conversely, any contrast-boosting prior needs to be non-Gaussian.

When computing posterior estimates, the unavoidable non-Gaussianity of any contrast-boosting prior, leads to computational complexity and high computational cost. In two-dimensional industrial tomography, with even small or moderate mesh sizes, a typical problem has around 100,000-1,000,000 unknown parameters. High-dimensionality in industry poses problems, especially in time-critical applications, where speed is valued. Optimisation methods are natural starting points as they are computationally less expensive. For example, maximum a posteriori (MAP) estimates, expectation-maximisation algorithm, and variational Bayesian methods are flavours of posterior analysis ([Tzikas et al., 2008](#)). They provide computational efficiency, but they do not provide full uncertainty quantification.

To fully quantify uncertainty, we need to explore the whole posterior, that is, use Markov chain Monte Carlo (MCMC) techniques. A straightforward choice is to use Metropolis-within-Gibbs (MwG), as the one given in [Markkanen et al. \(2019\)](#). There is a growing number of MCMC algorithms designed especially for high-dimensional problems ([Cotter et al., 2013](#); [Law, 2014](#); [Beskos et al., 2017](#)). Unfortunately, non-Gaussianity of the contrast-boosting priors breaks many of the assumptions of the function-space MCMC methods. For example, there is currently no preconditioned Crank-Nicolson algorithm for the pixel-based Cauchy prior constructions. MwG is a standard choice, but it typically

has some single, more problematic, pixels requiring significantly long MCMC chains. As an alternative, we shall use Hamiltonian Monte Carlo (HMC, Neal, 2011). It has been used for a wide range of applications and it is well-suited for large-dimensional problems (Beskos et al., 2011,0). In particular, we use the HMC variant with no-U-turn sampling (HMC-NUTS, Hoffman and Gelman, 2014).

There are several priors, which promote contrast-boosting or edge-preserving inversion. A standard choice for edge-preserving inversion are the total variation (TV) priors, which are based on using  $L^1$ -norms. In statistics, these methods are called LASSO. This method, however, has a drawback, which rises from the finiteness of the prior moments. When we make the discretisation denser and denser, the TV-priors converge to Gaussian priors in the discretisation limit. This behaviour was studied by Lassas and Siltanen (2004), and they showed that the estimators are not consistent under mesh refinement for Bayesian statistical inverse problems. This, naturally, means that doing uncertainty quantification under TV-prior assumption is not consistent with respect to the change of the mesh.

Recently, several hierarchical models, which promote more versatile behaviours, have been developed. These include, for example, deep Gaussian processes (Dunlop et al., 2018; Emzir et al., 2019), level-set methods (Dunlop et al., 2017), mixtures of compound Poisson processes and Gaussians (Hosseini, 2017), and stacked Matérn fields via stochastic partial differential equations (Roininen et al., 2019). The problem with hierarchical priors is that in the posteriors the parameters and hyperparameters may become strongly coupled, which means that vanilla MCMC methods become problematic and, for example, re-parameterisations are needed for sampling the posterior efficiently (Chada et al., 2019; Monterrubio-Gómez et al., 2019). In level-set methods, the number of levels is usually low, because experiments have shown that the method deteriorates when the number of levels is increased.

Here, we utilise a different approach, and make the prior non-Gaussian by construction without hierarchical modelling or compromising on uncertainty quantification. The first choice is to utilise priors based on Besov  $\mathcal{B}_{p,q}^s$  norms (Lassas et al., 2009). These priors are constructed on wavelet basis, typically Haar wavelets, and they have well-defined non-Gaussian discretisation limit behaviour. Besov priors have been utilised in a number of studies for Bayesian inversion, see, e.g., Niinimäki (2013). The problem with Besov priors is the structure of wavelets and the truncation of the wavelet series. The coefficients of the wavelets are random but actually not interchangeable, since their decay is necessary for convergence of the series. That typically means that we make an unnecessary and strong prior assumption for edge locations based on wavelet properties, for example, consider a one-dimensional inverse problem on domain  $(0,1)$ , we prefer an edge at  $1/4$  over an edge at  $1/3$  for Haar wavelets.

General  $\alpha$ -stable random field priors can be constructed with Karhunen-Loève (KL) expansions. For KL expansions, see Berliet and Thomas-Agnan (2004), and for stable field expansions, see Samorodnitsky and Taqqu (1994); Sullivan (2017). Third option is to use pixel-based approaches (Markkanen et al., 2019; Bolin, 2014; Mendoza et al., 2019), which cover also some  $\alpha$ -stable processes. As  $\alpha$ -stable processes, both KL-expansions and pixel-based approaches are valid, but one should note that the different approaches lead to different statistical objects. We stress that both approaches lead to well-posedness of the inverse problem. In this paper, we shall utilise certain pixel-based approaches, and limit the discussion to the Cauchy difference priors, which is a special case  $\alpha = 1$ .

### 1.3. Contribution and organisation of this work

The contributions of this paper are two-fold, first of all we make a large-scale numerical comparison for the X-ray tomography problem with different Gaussian and non-Gaussian (TV, Besov, Cauchy) prior assumptions. To the best of the authors' knowledge, this kind of comparison has not yet been published. Secondly, we apply a carefully designed HMC algorithm to the high-dimensional non-Gaussian inverse problem. In particular, we show its applicability for the sparse-angle tomography problem.

The rest of this paper is organised as follows: In Section 2, we review Gaussian, TV, Besov and Cauchy priors. In Section 3, we introduce the necessary MwG and HMC tools. In Section 4, we have two synthetic case studies: 3D-imaging of logs in sawmills, and drill-core tomography problem. Finally, in Section 5, we conclude the study, and make some notes on future developments.



## 2. Random field priors

For Gaussian, TV and Besov priors, we write the priors as  $\pi(X) \propto \exp(-G(X))$ , where  $G(X)$  is  $L^2$ -norm of differences of  $X$  for the Gaussian case,  $L^1$ -norm of differences for TV, and Besov  $\mathcal{B}_{p,q}^s$ -norm for a wavelet expansion with random coefficients  $X_1, \dots, X_m$  for Besov case. We will describe these distributions below and their respective  $G(X)$ . In the following, we will describe separately the Cauchy prior, as it is based on another type of construction.

### 2.1. Gaussian prior

Let us assume a zero-mean Gaussian prior, which is fully defined with one of the following choices,

$$G(X) = \frac{1}{2} X^T \Sigma^{-1} X = \frac{1}{2} X^T Q X = \frac{1}{2} X^T L^T L X = \frac{1}{2} (LX)^T L X,$$

where  $\Sigma$  is the covariance matrix,  $Q$  is the precision matrix and  $L$  is a square-root (e.g., Cholesky factor) of the precision matrix. Common choices are exponential and squared exponential covariances, Matérn covariances, and Brownian motion covariance. Different choices lead to different kinds of presentations, for example, squared exponential leads to full matrices for all  $\Sigma, Q, L$ , but with certain choices, the Matérn covariances have sparse  $Q, L$  matrices due to the Markov property (Roininen et al., 2019).

Two-dimensional difference priors can be obtained by choosing  $L$  to be a discretisation of the following operator equation  $\nabla X = \mathcal{W}$ , where  $\mathcal{W} = (\mathcal{W}_1, \mathcal{W}_2)^T$  with two statistically independent white noise random fields  $\mathcal{W}_1$  and  $\mathcal{W}_2$ . Thus we have  $LX = W$  for the discrete presentation, which we will solve in the least-squares sense. We note that the precision matrix  $Q = L^T L$  is not invertible, thus this is an improper prior, but if we impose zero-boundary conditions, we have a proper prior. For X-ray tomography zero-boundary conditions are natural choices, as typically the domain of interest is larger than the object of interest, and thus putting zero-boundary is justified. Now, let us denote by  $X_{i,j}$  the unknown at pixel  $(i, j)$ . As a summation formula with zero-boundary conditions, we can write the prior then as

$$G_{\text{Gauss}}(X) = G_{\text{pr}}(X) + G_{\text{boundary}}(X) = \sum_{i=1}^I \sum_{j=1}^J \left( \frac{(X_{i,j} - X_{i-1,j})^2}{\sigma_{\text{pr}}^2} + \frac{(X_{i,j} - X_{i,j-1})^2}{\sigma_{\text{pr}}^2} \right) + \sum_{i,j \in \partial\Omega} \frac{X_{i,j}^2}{\sigma_{\text{boundary}}^2},$$

where by  $\partial\Omega$  we mean the boundary indices of the discretised domain  $\Omega$ ,  $\sigma_{\text{pr}}^2$  is regularisation parameter, and  $\sigma_{\text{boundary}}^2$  zero-boundary parameter.

### 2.2. Total variation prior

Similarly to the Gaussian prior, we can write a two-dimensional TV prior with

$$G_{\text{TV}}(X) = G_{\text{pr}}(X) + G_{\text{boundary}}(X) = \sum_{i=1}^I \sum_{j=1}^J \alpha (|X_{i,j} - X_{i-1,j}| + |X_{i,j} - X_{i,j-1}|) + \sum_{i,j \in \partial\Omega} \alpha_{\text{boundary}} |X_{i,j}|,$$

where  $\alpha, \alpha_{\text{boundary}}$  are regularisation parameters. We note that in statistics, these distribution are often called Laplace distributions. This form of TV prior is anisotropic. According to González et al. (2017), it can be shown that an isotropic form is obtained when we choose

$$G_{\text{pr}}(X) = \sum_{i=1}^I \sum_{j=1}^J \alpha \left( (X_{i,j} - X_{i-1,j})^2 + (X_{i,j} - X_{i,j-1})^2 \right)^{1/2}.$$

Using higher-order TV priors would be possible (Liu *et al.*, 2015), but often the basic first order TV prior is selected because it preserves sharp edges within the reconstruction much better. The major drawback of TV prior is that due to its finite moments, the prior is not discretisation-invariant and it resembles Gaussian difference prior on dense enough meshes. It is notable that MAP estimate and the Conditional Mean (CM) estimate differ drastically of each other in the limit (Lassas and Siltanen, 2004). While the inconsistency is not desirable, the prior is still used in many practical applications. In the numerical experiments, we use anisotropic TV prior.

### 2.3. Besov prior

Gaussian and TV priors are based on Gaussian and Laplace distributions. Besov priors are based on wavelet coefficients of the reconstruction, and in practise calculated by discrete wavelet transform (DWT) (Lassas *et al.*, 2009). The continuous wavelet transform decomposes the reconstruction into approximation and detail coefficients. For detailed treatise on Besov priors, see (Niinimäki, 2013). Besov prior for  $X$  derives from wavelet expansion for function  $\mathcal{X}$

$$\mathcal{X} = \sum_{d_1=0}^{2^k-1} \sum_{d_2=0}^{2^k-1} \langle \mathcal{X}, \phi_{k,d_1,d_2} \rangle \phi_{k,d_1,d_2} + \sum_{r=k}^{\infty} \sum_{d_1=0}^{2^r-1} \sum_{d_2=0}^{2^r-1} \sum_{t=1}^3 \langle \mathcal{X}, \psi_{r,d_1,d_2,t} \rangle \psi_{r,d_1,d_2,t}, \quad (3)$$

and its Besov norm is

$$\|\mathcal{X}\|_{\mathcal{B}_{p,q}^s} = \left( \sum_{d_1=0}^{2^k-1} \sum_{d_2=0}^{2^k-1} |\langle \mathcal{X}, \phi_{k,d_1,d_2} \rangle|^p + \sum_{r=k}^{\infty} 2^{rq(s+1-2/p)} \sum_{d_1=0}^{2^r-1} \sum_{d_2=0}^{2^r-1} \sum_{t=1}^3 |\langle \mathcal{X}, \psi_{r,d_1,d_2,t} \rangle|^p \right)^{1/p}.$$

In Equation (3),  $\phi$  is the father wavelet and  $\psi$  is the mother wavelet. The subindices refer to different scales and translations of the functions (Meyer, 1992). We utilise the prior for Besov space  $\mathcal{B}_{1,1}^1$ , which reduces the norm into absolute sum of wavelet coefficients. Other Besov spaces than  $\mathcal{B}_{1,1}^1$  would be doable as well, but in those cases the wavelet coefficients would have different weights or they would be raised to other powers than one. We use Haar wavelets as our father and mother wavelets.

In practise, we compute the two-dimensional DWT of  $X$ , which is now represented as a reconstruction of size of  $2^n \times 2^n$ ,  $n \in \mathbb{N}$  square pixels. The Besov prior is defined by

$$G_{\text{Besov}}(X) = \sum_{d_1=0}^{2^k-1} \sum_{d_2=0}^{2^k-1} |a_{k,d_1,d_2}| + \sum_{r=k}^{k_{\max}} \sum_{d_1=0}^{2^r-1} \sum_{d_2=0}^{2^r-1} \sum_{t=1}^3 |b_{r,d_1,d_2,t}|.$$

Terms  $a_{k,d_1,d_2}$  refer to the approximation coefficients of the DWT of  $X$  and terms  $b_{r,d_1,d_2,t}$  to the corresponding detail coefficients. As DWT algorithm, we choose a matrix operator method described by Wang and Vieira (2010). A more common and faster way to calculate the DWT would be to use fast wavelet transform, but we want to keep track of how changing the value of an individual pixel alters the wavelet coefficients and therefore the prior, too. This property is needed in the MwG algorithm, because we propose new samples for each component of  $X$  in a sequential manner and calculating the whole DWT every time for all the components would be too time-consuming.

Besov priors are discretisation-invariant and therefore should remain consistent if the resolution is increased (Lassas *et al.*, 2009). Their drawback is the tendency to produce block artefacts into the point estimates: the wavelet coefficients at certain low scale are different, even though they are adjacent to each other. This makes Besov priors location-dependent, that is, they are not translation-invariant.

## 2.4. Cauchy prior

While the previous three priors were constructed based on different types of norms, Cauchy priors are constructed based on Cauchy walk, or more profoundly general  $\alpha$ -stable random walk. These one-dimensional objects have well-defined limits, and the generalisation in (Markkanen et al., 2019) to two-dimensional setting is given as a prior density

$$\pi(X) \propto \prod_{i=1}^I \prod_{j=1}^J \frac{h\lambda}{(h\lambda)^2 + (X_{i,j} - X_{i-1,j})^2} \frac{h\lambda}{(h\lambda)^2 + (X_{i,j} - X_{i,j-1})^2},$$

where  $h$  is discretisation step in both coordinate directions, and  $\lambda$  is the regularisation parameter. These priors have been used for X-ray tomography in oil and gas industry (Mendoza et al., 2019) and subsurface imaging (Muhumuza et al., 2019).

A second formulation of the Cauchy difference prior was derived in (Chada et al., 2019). In that, the starting point was  $\alpha$ -stable sheets, which lead to difference approximations of the form

$$\pi(X) \propto \prod_{i=1}^I \prod_{j=1}^J \frac{h^2\lambda}{(h^2\lambda)^2 + (X_{i,j} - X_{i-1,j} - X_{i,j-1} + X_{i-1,j-1})^2}.$$

We note that Cauchy difference prior is theoretically justified in the discretisation limit, which is not the case with TV prior. Unlike Gaussian difference prior, Cauchy difference prior favours small increments and steep transitions relatively much more. This means that Cauchy difference prior preserves edges within the lattice and does not smooth them out. A disadvantage of Cauchy difference prior is its anisotropic nature.

## 3. Posterior estimates

The two most common estimators drawn from the posterior density (2) are the MAP and CM estimates. For MAP estimation, we will use Limited-memory BFGS (L-BFGS) optimisation algorithm, which belongs to the family of quasi-Newtonian methods. For CM estimation, we shall use MCMC methods, as they also enable uncertainty quantification of the estimators.

### 3.1. Adaptive Metropolis-within-Gibbs

We shall use single-component adaptive Metropolis-Hastings (SCAM) (Haario et al., 2005) to generate samples from the posterior distributions. It is an adaptive variation of the MwG algorithm, which is a generalisation of Gibbs sampling. In Gibbs sampling, the samples are generated by generating new values for each component of the target distribution from the component-wise conditional distributions. However, if it is not possible to obtain samples from such distributions analytically, MwG can be used instead, since it utilises Metropolis-Hastings acceptance/rejection step for proposing new values for the components. In theory, both methods are applicable also in very high-dimensional distributions.

The adaptive MwG algorithm adapts a Gaussian transition kernel for each component during the burn-in period. This means that algorithm calculates the variance of each component in the chain and sets new proposal variances for them. By this way, the algorithm does not require manual tuning, unlike the non-adaptive MwG algorithm does. We note that self-adaptation does not fix the fundamental problem of component-wise sampling – the algorithm is unable to sample from distributions, which support consists of diagonally separated regions, since the algorithm cannot jump from one region to another without transforming the coordinate system of the distribution. If the distribution is heavy-tailed, the variance-based adaptation might not converge to a reasonable proposal variance at all because the conditional distributions have infinite or undefined variances. Single component robust adaptive

Metropolis-Hastings (RAM) (Vihola, 2011) tunes the proposal variance according to the acceptance ratio of each component so far in the chain and hence should work better with heavy-tailed distributions. Furthermore, strong correlations in high-dimensional distributions might impair the sampling efficiency of component-wise samplers.

Another feature of MwG is that since the candidate generating kernel is centred at the previous sample and no matter what the proposal covariance is, there will be significant correlation between the samples in the chain. This decreases the effective sample size of the generated samples, since they are not actually independently drawn from the target distribution.

### 3.2. Hamiltonian Monte Carlo

Here, we will summarise the Hamiltonian Monte Carlo (HMC, Neal, 2011) method. For an expanded conceptual descriptions of the HMC, the reader is directed to Betancourt (2017). In HMC, the geometric information of the typical set is used to guess of a new sample location. The Hamiltonian dynamic is used in to determine the path between the current sample position and the next sample. Specifically, one considers the negative logarithm of the probability density function of the target distribution as a potential energy function (Neal, 2011; Barp *et al.*, 2018). Then one introduces an auxiliary momentum  $P$  and kinetic energy function  $K(P)$  with suitable mass matrix  $M$ , which are used along with the potential energy function to form the Hamiltonian function:

$$H(X, P) = U(X) + K(P) = -\log(P) + K(P) = -\log(P) + \frac{P^T M^{-1} P}{2}.$$

In order to sample from the target distribution, one starts following a Hamiltonian trajectory from the previous sample in the chain by setting  $X^* = X_{k-1}$  and by sampling a momentum vector from its proposal distribution. Then, one approximates the following Hamiltonian equations with a symplectic integrator, like Störmer-Verlet:

$$\frac{\partial H(X^*, P)}{\partial P} = \frac{dX^*}{dt}, \quad \frac{\partial H(X^*, P)}{\partial X^*} = -\frac{dP}{dt}.$$

As Hamiltonian is time-reversible and the trajectories preserve their volume in the phase space, the new proposal sample can be selected to be the last value of  $X^*$  at the end of the trajectory. The final step is to apply a Metropolis acceptance/rejection step to correct for the numerical approximation error caused by time discretisation. The computational complexity of generating the samples scales with  $m^{\frac{5}{4}}$  (Beskos *et al.*, 2013), whereas random walk Metropolis-Hastings algorithms scale with  $m^2$  (Neal, 2011).

Selecting appropriate step size of the symplectic integrator and the corresponding trajectory length is apparent problems of the basic HMC. If the step size is too big, the value of Hamiltonian is not preserved so precisely and most of the proposals are rejected. If it is too small, the extra computational burden makes the algorithm impractically slow. Also, too long overall trajectory length both wastes time and actually increases the change that the trajectory comes close to the initial state, whereas too short trajectory evidently means that the trajectory always ends near the starting point. A self-adaptive HMC algorithm No-U-Turn Sampler (NUTS) adapts the integration step size by changing its value with respect to acceptance ratio so far in the chain by routine called Dual Averaging (Hoffman and Gelman, 2014). NUTS does not use a fixed trajectory length, since it calculates the trajectory randomly in the opposite directions from the starting point. Furthermore, it uses a set of heuristics to remain the reversibility and to stop simulating trajectories until they start to turn back. These facts render NUTS a promising method for sampling from high-dimensional distributions with possibly severe correlations. However, even NUTS might need setting an appropriate mass matrix to sample efficiently from the target distribution. One way to select a mass matrix is to run preliminary MCMC chains to calculate an

empirical covariance for the distribution and use it as the mass matrix. If the distribution is very high-dimensional, the mass matrix might be just diagonal. More sophisticated approach is to utilise mass matrices, which are not constant. That is the case in Riemannian Manifold HMC algorithms (Girolami and Calderhead, 2011).

#### 4. Numerical experiments

We have two numerical experiments, the log tomography and the drill-core tomography. The measurement setting is the same for both test cases: We shall use X-ray tomography with parallel beam geometry. The computational grid is  $512 \times 512$ , so we have 262,144-dimensional posterior distributions. We have additive white noise models, according to Equation (1), we fix the standard deviation of the noise to 1.5% of the maximum value of the line integrals. The parameters of each prior distribution at each measurement scenario are set using a grid search. We select the parameter value, which gives approximately a minimum  $L^2$ -error between the MAP estimate given by the parameter value and the ground truth. Furthermore, in the log tomography case, we use a different log slice without a high density object to select the parameters by the grid search. For Besov prior, we use 8 levels in the DWT.

For log tomography, we have a foreign object inside, thus it is a high-contrast target. The second experiment is a lower-contrast target with lots of distinct regions with different attenuation coefficient. In simulations, we shall use the four priors, L-BFGS, adaptive MwG, and HMC-NUTS. The initial points of MCMC chains are set to be the MAP estimate obtained with L-BFGS. As MCMC chain lengths, we use 500,000 samples in MwG to adapt a proposal variance for each component and we use those variances to generate 400,000 samples to calculate CM estimates. For NUTS, we let the algorithm run 100 times, at which time the dual averaging algorithm adapts a step length for the Störmer-Verlet symplectic integrator. Then we use that step length to generate 4,000 samples for CM estimates.

##### 4.1. Log tomography

Our test case is visualised in Figure 1, with metallic piece in black and knots in light color, and a small rotten part in near white with more smooth behavior. Besides the ground truth, we have also plotted the three-dimensional estimates, obtained by stacking two-dimensional MAP estimate slices computed with L-BFGS. We have all the four different priors, and the number of equispaced measurement angles is 10, 30 or 90. While all the methods seem to capture the main features in densest-data case, reducing the number of measurement leads to severe artefacts with Gaussian and TV priors, and the Besov prior promotes blocky estimate. Cauchy prior seems to capture the metallic piece even in the most difficult case, but it struggles with knots.

It is easier to see the effects of different priors in the two-dimensional slices in Figure 2. The densest scenario, with 90 angles, TV and Cauchy priors produce very good MAP estimates recovering the edges. MAP estimate with Besov prior looks blocky. In the MAP estimate with Gaussian prior, the edges of the metallic object are smoothed. Reducing the number of measurement angles causes visible artefacts into MAP-estimates with TV and Gaussian priors, but TV prior preserves the edges much better. Meanwhile, the rotation-dependency of Cauchy difference prior becomes apparent with coordinate-axis aligned sharp artefacts. The Besov prior MAP estimate remains more or less consistent even if the number of angles is decreased. However, in practice the block artefacts will spoil the MAP estimates and that is not useful in practical applications. We could decrease the number of wavelet transform levels in order to reduce blockiness, or use another wavelet family.

In Figure 3, we have plotted the CM estimates computed with MwG and HMC. Here we skip Gaussian priors, as the CM and MAP estimates with Gaussian priors are the same. It is notable that the CM estimate with TV prior differs noticeably from its MAP estimate (Figures 1 and 2). For high-dimensional inverse problems, it has been demonstrated by Lassas and Siltanen (2004, Figure 4) that

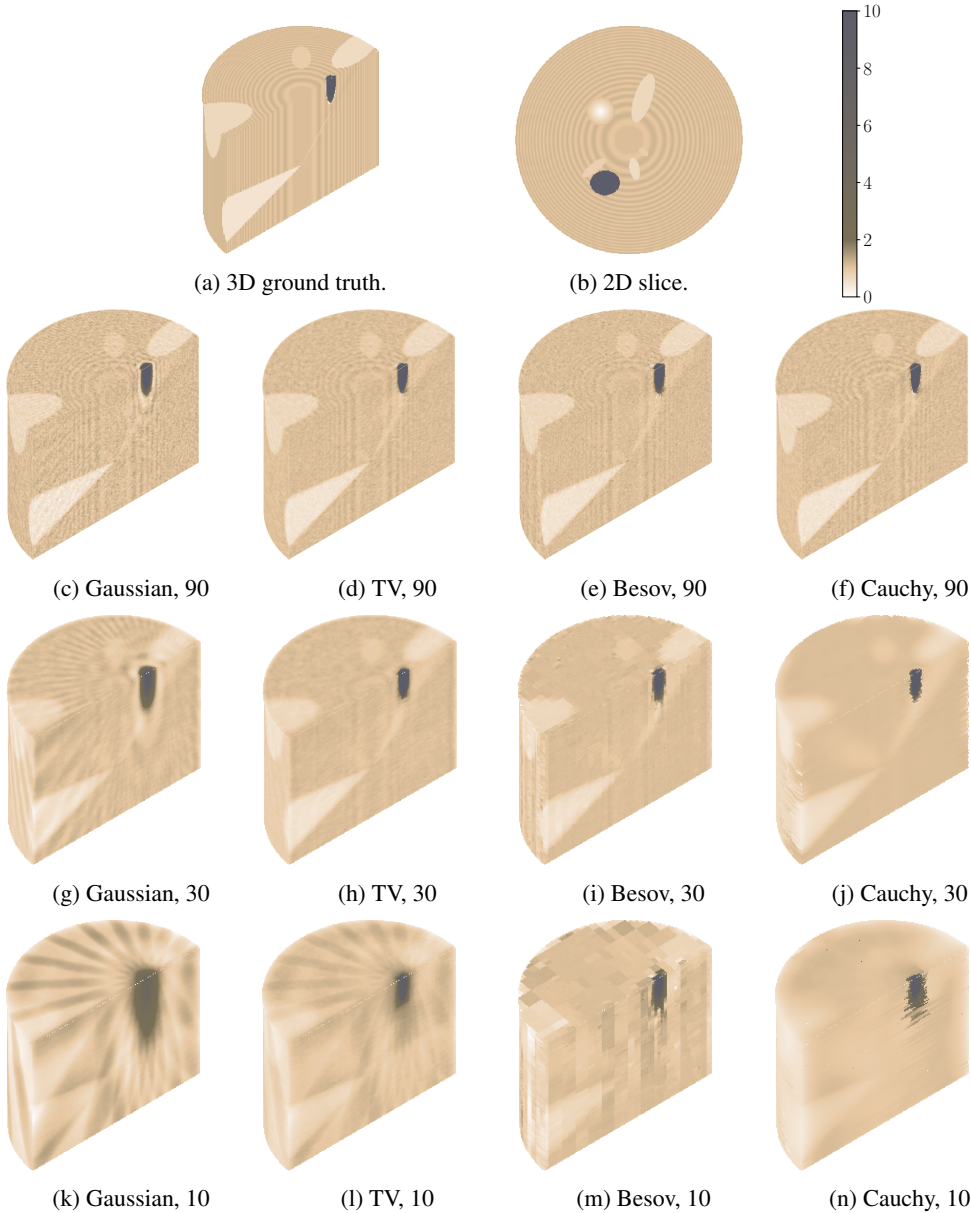


**Figure 1.** Three-dimensional ground truth and two-dimensional ground truth with knots (light material) and metallic piece (black). Three-dimensional reconstructions obtained by stacking two-dimensional MAP estimates with different angles and priors.

CM estimates might be wildly oscillatory, even though the same prior produces reasonable MAP estimates. Also, the great number of scanning artefacts is notable. On the other hand, CM estimates with Cauchy difference prior have less coordinate-axis related artefacts, and CM estimates of Besov prior are less blocky than their corresponding MAP estimates.

In Figure 4, we have logarithmic pixel-wise variances estimated from the MCMC chains with MwG and HMC-NUTS. For TV and Besov priors, MwG and HMC produce similar results. However, they produce different variance estimates for Cauchy prior at the 30 angle case. This is because some of the pixels at the boundary of the high density object have much higher variance than the other boundary pixels. This is a mixing issue, and we notice that with heavy tails the MwG and HMC require longer



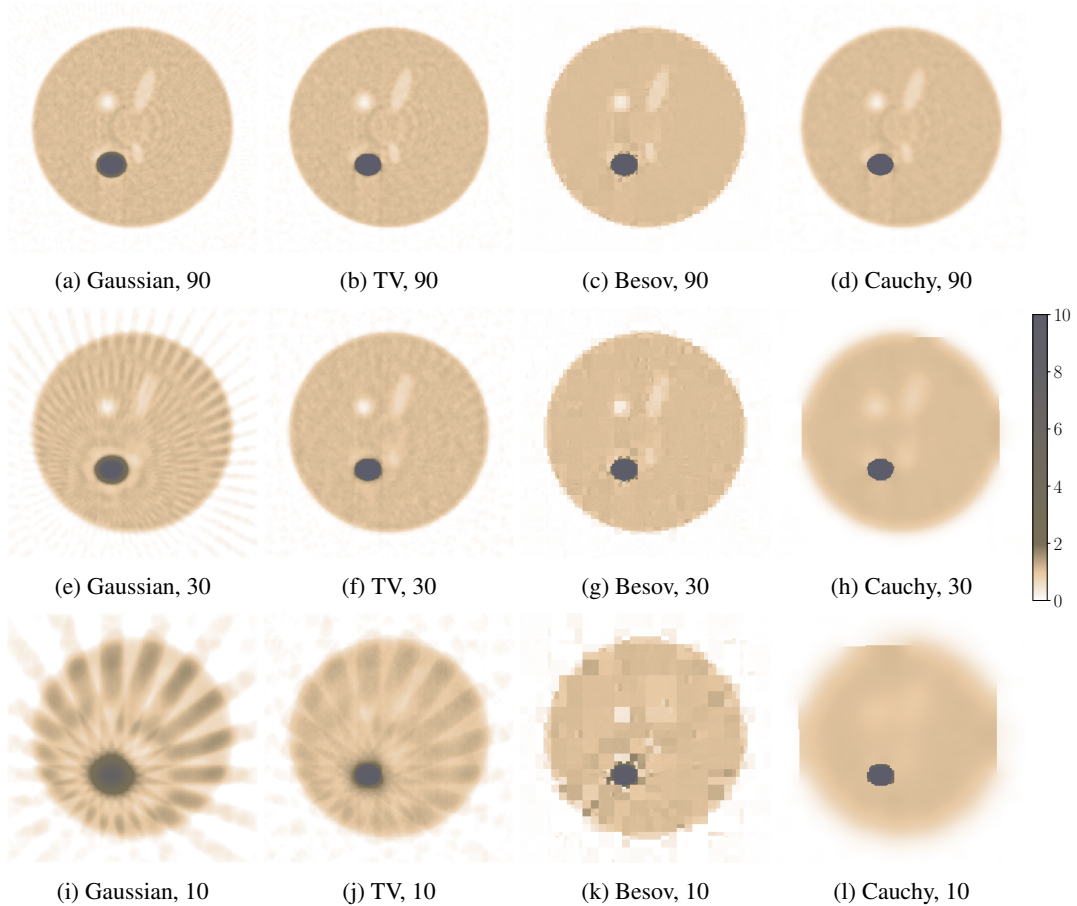


**Figure 2.** Two-dimensional MAP estimates with different measurement angles and prior assumptions.

chains for Cauchy than for TV and Besov. We could improve the sampling capabilities of NUTS by adapting a diagonal global mass matrix different than the identity one by running a preliminary run to estimate the variance of posterior. Adapting a full covariance matrix or using a local metric and therefore changing HMC-NUTS to Riemannian Manifold Monte Carlo would be computationally infeasible in this kind of a high-dimensional case. On the other hand, there is not much we can do to improve the space exploration in MwG. We might change the adaptation strategy to the component-wise robust adaptive Metropolis-Hastings, which should explore the heavy tails more efficiently.

#### 4.2. Drill-core tomography

Here we take a simpler setting for a lower-contrast target, and we detect pores and mineralised soil within a core sample. Unlike in the log tomography experiment, there are no objects with drastically different absorption coefficient than the surrounding matter has in the domain of interest. However, the drill-core sample has lots of pores and soil cobs and their sizes also vary.

We shall only demonstrate MAP estimation, and the results are in Figure 5. At the first glance, there are no significant differences within the MAP estimates if we compare TV, Cauchy and Gaussian difference priors to each other at 90 measurement angle scenario. Nevertheless, we consider the Cauchy and TV priors as the best ones, since they have the least amount of noise present and they still preserve the edges of the pores with low density and denser regions of the core sample well. If we wanted

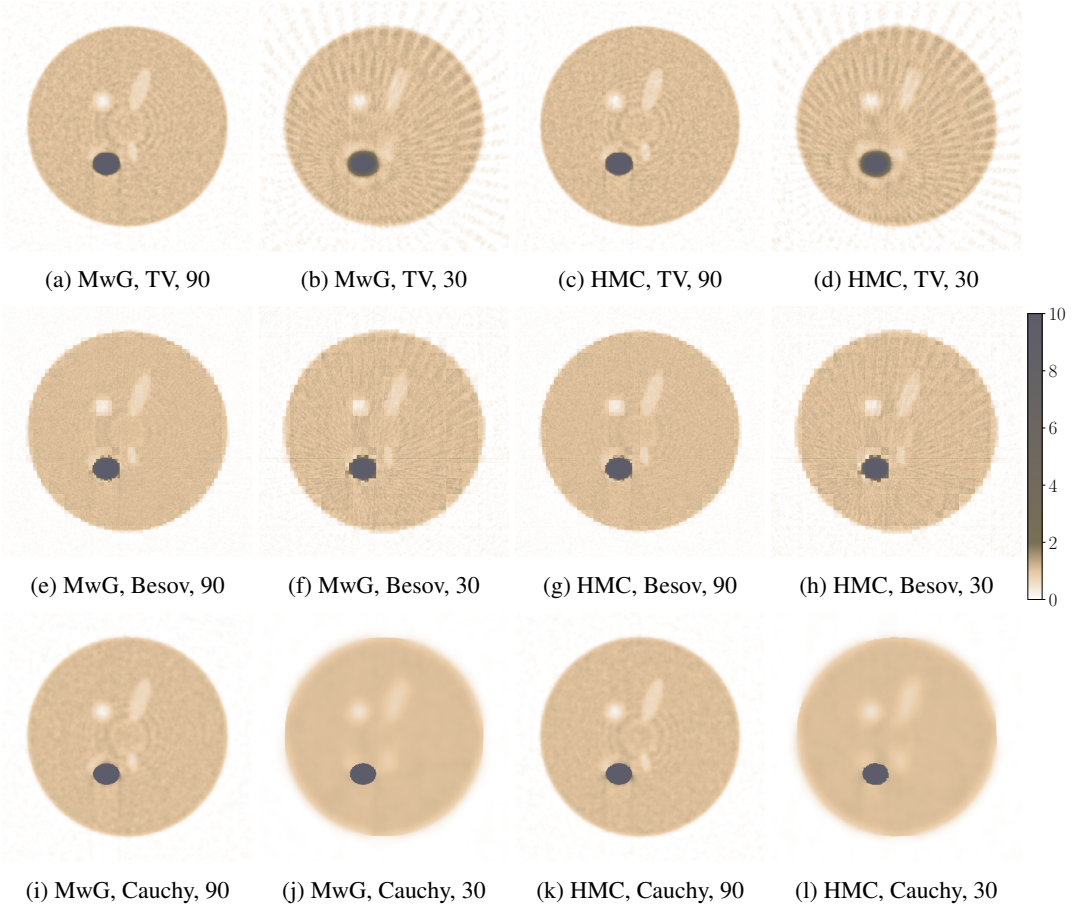


**Figure 3.** Two-dimensional CM estimates with different measurement angles, prior assumptions, and samplers.

to achieve the same level of noise with Gaussian difference prior, we would end up having clearly oversmoothed MAP estimates.

At the 30 angle measurement angle scenario, MAP estimate with Besov prior is severely ruined with block artefacts and in the 10 angle scenario, it is completely useless. This is likely due to the fact that the region of interest consists of many spherical objects which are close to each other, but the wavelet coefficients of Haar family do not approximate well such details. Unlike in the log tomography case, there are not so many artefacts present in the MAP estimates calculated with Gaussian prior. In the 10 angle case, MAP estimates calculated with Gaussian, TV and Cauchy priors are very close to each other and neither of them can be considered superior over the others. We could try to fix the coordinate-axis dependency of Cauchy prior by introducing isotropic Cauchy prior so that we set a bivariate Cauchy distribution for differences of each pixel to their neighbours.

## 5. Conclusion

We have made a Bayesian inversion industrial tomography comparison study with four different prior assumptions. The targets have different contrasts, that is, sharp edges were to be reconstructed. This is a classical problem, where one needs either hierarchical or non-Gaussian models, and hence inherently computational complexity becomes a problem. The chosen methods, to use optimisation or MCMC, is a balance between fast computations and uncertainty quantification. It should be noted that for many

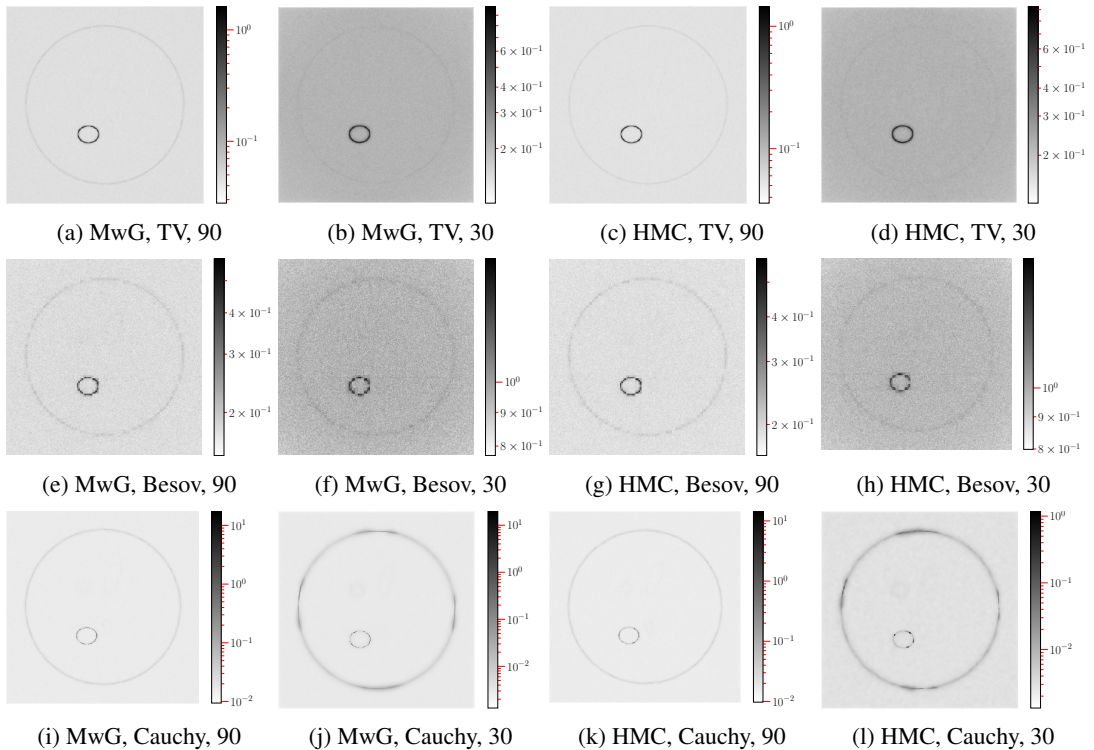


**Figure 4.** Pixel-wise variance estimates for the CM estimates in Figure 3.

industrial applications the computational cost is still too high for many dynamical systems. However, for static objects and case studies where computational time is not critical, the correctly chosen methods can significantly enhance the reconstruction results for difficult measurement geometries and targets. It is notable that systematic choices of different parameters, including mesh refinement parameters, dictate the reconstruction accuracy. Here, we have used simple grid searches, in order to show the maximum possible reconstruction capabilities of the priors while paying attention to which kind of artefacts each prior had. In reality, choosing the parameters would require implementing some kind of a hierarchical model. This would naturally further increase computational complexity.

In all the scenarios we considered, MAP estimates with Cauchy and TV priors were considered the best – their artefacts were mild in general and, while their edge-preserving performances were still excellent. The point estimates using Besov prior with at least Haar wavelets underperformed remarkably compared to the other priors in most cases due to the major block artefacts it tends to produce. We could reduce that behaviour by reducing the number of DWT levels and using another wavelet family, but even that cannot improve the location-dependency of the prior. Likewise, we could try fixing the anisotropic of the Cauchy prior with a bivariate Cauchy distribution or using the alternative formulations of the prior. For further development, acceptance-ratio-based adaptation in MwG and setting a non-identity mass matrix for HMC would improve sampling.

Further improvements in addition to the aforementioned ones, we should consider using other prior distributions, like general  $\alpha$ -stable priors, or using hierarchical priors. For instance, instead of the Gaussian prior we might test various hierarchical Gaussian priors with possible many layers to potentially improve the edge-preserving properties of it.

**Acknowledgments.** Authors thank Prof. Heikki Haario and Prof. Marko Laine for useful discussions.

**Funding statement.** This work has been funded by Academy of Finland (project numbers 326240, 326341, 314474, 321900, 313708) and by European Regional Development Fund (ARKS project A74305).

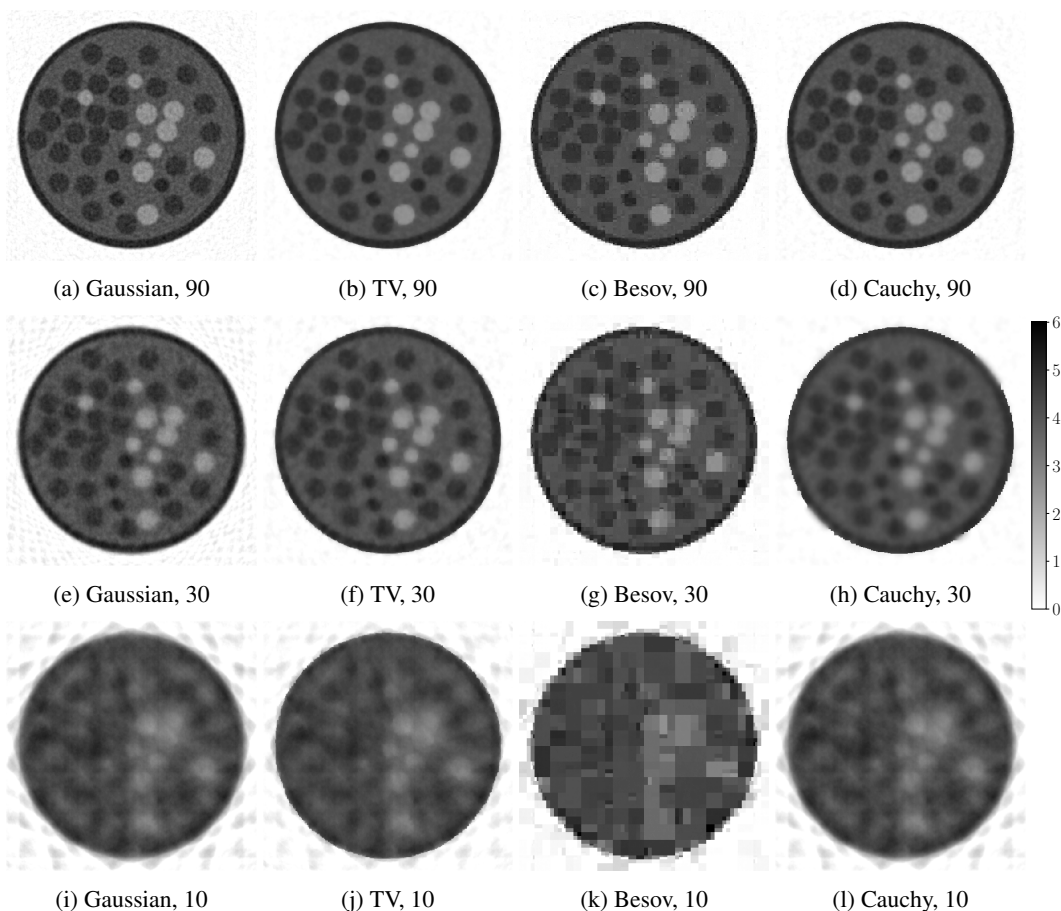


**Figure 5.** MAP estimates for the drill-core experiment with different measurement angles and prior assumptions.

**Competing interests.** None.

**Data availability statement.** Codes and the synthetic data used are available openly in GitHub <https://github.com/suurj/tomo/>.

**Ethical standards.** We have followed the ethical code of conduct for research and publication of the Academy of Finland.

**Author contributions.** Conceptualisation: S.L.; S.S.; L.R. Funding acquisition: S.S.; L.R. Methodology: J.S.; M.E.; S.L.; S.S.; L.R. Data visualisation: J.S. Software: J.S.; M.E. Writing original draft: J.S.; M.E.; S.L.; L.R. All authors approved the final submitted draft.

**Supplementary material.** None.

## References

- Bardsley, J. (2012). MCMC-Based Image Reconstruction with Uncertainty Quantification. *SIAM Journal on Scientific Computing*, 34.
- Bardsley, J. (2013). Gaussian Markov random field priors for inverse problems. *Inverse Problems and Imaging*, 7:397–416.
- Barp, A., Briol, F.-X., Kennedy, A. D., and Girolami, M. (2018). Geometry and dynamics for Markov chain Monte Carlo. *Annual Review of Statistics and Its Application*, 5(1):451–471.
- Berlinet, A. and Thomas-Agnan, C. (2004). *Reproducing kernel Hilbert spaces in probability and statistics*. Kluwer Academic Publishers, Boston, MA. With a preface by Persi Diaconis.
- Beskos, A., Girolami, M., Lan, S., Farrell, P. E., and Stuart, A. M. (2017). Geometric MCMC for infinite-dimensional inverse problems. *J. Comp. Phys.*, 335:327–351.

- Beskos, A., Pillai, N., Roberts, G., Sanz-Serna, J.-M., and Stuart, A. (2013). Optimal tuning of the hybrid Monte Carlo algorithm. *Bernoulli*, 19(5A):1501–1534.
- Beskos, A., Pinski, F. J., Sanz-Serna, J. M., and Stuart, A. (2011). Hybrid Monte Carlo on Hilbert spaces. *Stochastic Processes and their Applications*, 121(10):2201–2230.
- Betancourt, M. (2017). A Conceptual Introduction to Hamiltonian Monte Carlo. *arXiv preprint, arXiv:1701.02434*.
- Bolin, D. (2014). Spatial Matérn fields driven by non-Gaussian noise. *Scandinavian Journal of Statistics*, 41:557–579.
- Chada, N. K., Lasanen, S., and Roininen, L. (2019). Posterior convergence analysis of  $\alpha$ -stable sheets. *arXiv preprint, arXiv:1907.03086*.
- Cotter, S. L., Roberts, G. O., Stuart, A. M., and White, D. (2013). MCMC methods for functions: Modifying old algorithms to make them faster. *Statistical Science*, 28(3):424–446.
- Dunlop, M. M., Girolami, M. A., Stuart, A. M., and Teckentrup, A. L. (2018). How deep are deep Gaussian processes? *Journal of Machine Learning Research*, 19(54):1–46.
- Dunlop, M. M., Iglesias, M. A., and Stuart, A. M. (2017). Hierarchical Bayesian level set inversion. *Statistics and Computing*, 27:1555–1584.
- Emzir, M. F., Lasanen, S., Purisha, Z., and Särkkä, S. (2019). Hilbert-space reduced-rank methods for deep Gaussian processes. In *2019 IEEE 29th International Workshop on Machine Learning for Signal Processing (MLSP)*. IEEE.
- Ernst, J. R., Green, A. G., Maurer, H., and Holliger, K. (2007). Application of a new 2d time-domain full-waveform inversion scheme to crosshole radar data. *GEOPHYSICS*, 72(5):J53–J64.
- Garcea, S., Wang, Y., and Withers, P. (2018). X-ray computed tomography of polymer composites. *Composites Science and Technology*, 156:305 – 319.
- Girolami, M. and Calderhead, B. (2011). Riemann manifold Langevin and Hamiltonian Monte Carlo methods. *Journal of the Royal Statistical Society: Series B (Statistical Methodology)*, 73(2):123–214.
- González, G. (2017). *Edge-promoting priors in electrical impedance tomography*. PhD thesis, University of Eastern Finland.
- González, G., Kolehmainen, V., and Seppänen, A. (2017). Isotropic and anisotropic total variation regularization in electrical impedance tomography. *Computers & Mathematics with Applications*, 74:564–576.
- Haario, H., Saksman, E., and Tamminen, J. (2005). Componentwise adaptation for high dimensional MCMC. *Computational Statistics*, 20:265–273.
- Hoffman, M. D. and Gelman, A. (2014). The no-u-turn sampler: Adaptively setting path lengths in Hamiltonian Monte Carlo. *Journal of Machine Learning Research*, 15:1593–1623.
- Hosseini, B. (2017). Well-posed Bayesian inverse problems with infinitely divisible and heavy-tailed prior measures. *SIAM/ASA Journal on Uncertainty Quantification*, 5:1024–1060.
- Huai, N., Zeng, Z., Li, J., Zhao, X., Liu, C., and Liu, F. (2016). Ground penetrating radar detection and parameter inversion of metalliferous veins based on stochastic effective media model. pages 1–6.
- Kaipio, J. and Somersalo, E. (2005). *Statistical and Computational Inverse Problems*. Springer, Dordrecht.
- Kruth, J.-P., Bartscher, M., Carmignato, S., Schmitt, R., Chiffre, L., and Weckenmann, A. (2011). Computed tomography for dimensional metrology. *CIRP Annals-manufacturing Technology - CIRP ANN-MANUF TECHNOLOGY*, 60:821–842.
- Lassas, M., Saksman, E., and Siltanen, S. (2009). Discretization-invariant Bayesian inversion and Besov space priors. *Inverse Problems and Imaging*, 3(1):87–122.
- Lassas, M. and Siltanen, S. (2004). Can one use total variation prior for edge-preserving Bayesian inversion? *Inverse Problems*, 20(5):1537–1563.
- Law, K. J. H. (2014). Proposals which speed up function-space MCMC. *Journal of Computational and Applied Mathematics*, 262:127–138. Selected Papers from NUMDIFF-13.
- Liu, J., Huang, T.-Z., Selesnick, I. W., Lv, X.-G., and Chen, P.-Y. (2015). Image restoration using total variation with overlapping group sparsity. *Information Sciences*, 295:232–246.
- Markkanen, M., Roininen, L., Huttunen, J. M. J., and Lasanen, S. (2019). Cauchy difference priors for edge-preserving Bayesian inversion. *Journal of Inverse and Ill-posed Problems*, 27(2):225–240.
- Mendoza, A., Roininen, L., Girolami, M., Heikkinen, J., and Haario, H. (2019). Statistical methods to enable practical on-site tomographic imaging of whole-core samples. *Geophysics*, 84(3):D89–D100.
- Meyer, Y. (1992). *Wavelets and operators*, volume 37 of *Cambridge Studies in Advanced Mathematics*. Cambridge University Press, Cambridge. Translated from the 1990 French original by D. H. Salinger.
- Monterrubio-Gómez, K., Roininen, L., Wade, S., Damoulas, T., and Girolami, M. (2019). Posterior inference for sparse hierarchical non-stationary models. *arXiv preprint, arXiv:1804.01431*.
- Muhumuza, K., Roininen, L., Huttunen, J. M. J., and Lähivaara, T. (2019). A Bayesian-based approach to improving acoustic Born waveform inversion of seismic data for viscoelastic media. *arXiv preprint, arXiv:1911.01192*.
- Natterer, F. (2001). *The Mathematics of Computerized Tomography (Classics in Applied Mathematics)*. SIAM: Society for Industrial and Applied Mathematics.
- Neal, R. (2011). MCMC using Hamiltonian dynamics. In *Handbook of Markov Chain Monte Carlo*, chapter 5, pages 113–162. CRC Press.
- Niinimäki, K. (2013). *Computational Optimization Methods for Large-scale Inverse Problems*. PhD thesis, University of Eastern Finland.



- Ou, X., Zhang, X., Lowe, T., Blanc, R., Rad, M. N., Wang, Y., Batail, N., Pham, C., Shokri, N., Garforth, A. A., Withers, P. J., and Fan, X. (2017). X-ray micro computed tomography characterization of cellular sic foams for their applications in chemical engineering. *Materials Characterization*, 123:20 – 28.
- Piao, Z.-y., Zhou, Z.-y., Xu, J., and Wang, H.-d. (2019). Use of X-ray Computed Tomography to Investigate Rolling Contact Cracks in Plasma Sprayed Fe-Cr-B-Si Coating. *TRIBOLOGY LETTERS*, 67(1).
- Roininen, L., Girolami, M., Lasanen, S., and Markkanen, M. (2019). Hyperpriors for Matérn fields with applications in Bayesian inversion. *Inverse Problems and Imaging*, 13(1):1–29.
- Rotella, A., Nadot, Y., Piellard, M., Augustin, R., and Fleuriot, M. (2018). Fatigue limit of a cast al-si-mg alloy (a357-t6) with natural casting shrinkages using astm standard x-ray inspection. *International Journal of Fatigue*, 114:177 – 188.
- Samorodnitsky, G. and Taqqu, M. S. (1994). *Stable non-Gaussian random processes*. Stochastic Modeling. Chapman & Hall, New York. Stochastic models with infinite variance.
- Shustrov, D., Eerola, T., Lensu, L., Kälviäinen, H., and Haario, H. (2019). Fine-grained wood species identification using convolutional neural networks. In Felsberg, M., Forssén, P.-E., Sintorn, I.-M., and Unger, J., editors, *Image Analysis*, pages 67–77, Cham. Springer International Publishing.
- Siltanen, S., Kolehmainen, V., Järvenpää, S., Kaipio, J., Koistinen, P., Lassas, M., Pirttilä, J., and Somersalo, E. (2003). Statistical inversion for medical x-ray tomography with few radiographs: I. General theory. *Physics in Medicine and Biology*, 48(10):1465–1490.
- Sullivan, T. J. (2017). Well-posed Bayesian inverse problems and heavy-tailed stable quasi-Banach space priors. *Inverse Problems and Imaging*, 11(5):857–874.
- Thanh, D., Prasath, S., and Le Minh, H. (2019). A Review on CT and X-Ray Images Denoising Methods. *Informatica*, 43:151–159.
- Toft, P. (1996). *The Radon Transform - Theory and Implementation*. PhD thesis, Technical University of Denmark.
- Tzikas, D., Likas, A., and Galatsanos, N. (2008). The Variational Approximation for Bayesian Inference Life after the EM algorithm. *Signal Processing Magazine, IEEE*, 25:131 – 146.
- Vihola, M. (2011). Robust adaptive Metropolis algorithm with coerced acceptance rate. *Statistics and Computing*, 22(5):997–1008.
- Villarraga-Gómez, H., Herazo, E. L., and Smith, S. T. (2019). X-ray computed tomography: from medical imaging to dimensional metrology. *Precision Engineering*, 60:544 – 569.
- Wang, H. and Vieira, J. (2010). 2-D wavelet transforms in the form of matrices and application in compressed sensing. In *2010 8th World Congress on Intelligent Control and Automation*, pages 35–39.
- Whiting, B. R. (2002). Signal statistics in x-ray computed tomography. In *Medical Imaging 2002: Physics of Medical Imaging*, volume 4682, pages 53–60. International Society for Optics and Photonics.
- Zolotarev, F., Eerola, T., Lensu, L., Kälviäinen, H., Haario, H., Heikkinen, J., and Kauppi, T. (2019). Timber tracing with multimodal encoder-decoder networks. In Vento, M. and Percannella, G., editors, *Computer Analysis of Images and Patterns*, pages 342–353, Cham. Springer International Publishing.